Elastic behaviour of an edge dislocation near a sharp crack emanating from a semi-elliptical blunt crack*

Fang Qi-Hong(方棋洪)†, Song Hao-Peng(宋豪鹏), and Liu You-Wen(刘又文)

College of Mechanics and Aerospace, Hunan University, Changsha 410082, *China*

(Received 26 October 2008; revised manuscript received 3 July 2009)

The interaction between an edge dislocation and a crack emanating from a semi-elliptic hole is dealt with. Utilizing the complex variable method, closed form solutions are derived for complex potentials and stress fields. The stress intensity factor at the tip of the crack and the image force acting on the edge dislocation are also calculated. The influence of the morphology of the blunt crack and the position of the edge dislocation on the shielding effect to the crack and the image force is examined in detail. The results indicate that the shielding or anti-shielding effect to the stress intensity factor increases acutely when the dislocation approaches the tip of the crack. The effect of the morphology of the blunt crack on the stress intensity factor of the crack and the image force is very significant.

Keywords: edge dislocation, blunt crack, shielding effect, image force

PACC: 6170G, 6220M, 4630N

1. Introduction

It is well known that dislocations in the vicinity of a crack tip play an important role in fracture mechanics. Therefore, the elastic interaction between dislocations and cracks has been extensively studied by many theoretical and experimental researchers.[1−10] The stress field, image force and strain energy of dislocation, and the stress intensity factor at the crack tip are the major concerns in these investigations. When plastic deformation has occurred around a crack tip, the stress field in the vicinity of the tip alters. One of the mechanisms, the dislocation emitted from the crack tip into the plastic zone, can reduce the stress intensity factor at the crack tip. This phenomenon is known as the dislocation shielding effect.[11] Apart from the dislocation shielding effect, crack blunting is another important mechanism which can reduce the stress field around the crack tip. Hence, the interaction between dislocations and blunt cracks has prompted many investigations. Lung and Wang[12] and Lee[13] simulated a blunt crack by an elliptic hole and calculated the image force acting on the screw dislocation near the blunt crack tip. Chen *et al.*[14] analysed the stress field, image force and shielding effect of an edge dislocation in the vicinity of an elliptical hole. Fischer and Beltz[15] examined the effect of crack blunting on the competition between dislocation emission and cleavage for an elliptical notch under mode I loadings. Qian *et al.*[16] calculated the stress distribution ahead of a blunt crack tip after dislocation emission. Huang and Li[17] obtained an explicit solution for prediction of the critical stress intensity factor (SIF) for edge dislocation emission from a blunt crack tip under mode I and II loading conditions. The shielding effect of the screw dislocation on an elliptically blunted crack is discussed by Li *et al.*[18] The shielding effect and emission criterion of a screw dislocation near an interfacial blunt crack is studied by Song *et al.*[19] In addition, the behaviour of an extended dislocation near an elliptical blunt crack is also investigated by Song *et al.*[20]

On the other hand, Vehoff and Neumann[21] provided experimental evidence that the crack widens as it propagates, but its tip still remains sharp. In addition, Ohr[22] also provided experimental evidence that the emission of a dislocation from a crack tip results in crack blunting. When the crack is blunted to a certain extent, the emission of dislocations from a crack tip can be interrupted. The blunted crack will not propagate until the nucleation of a new sharp crack. The dislocation may be re-emitted from a sharp crack emanating from the blunt crack. Therefore, Shiue and Lee,[23,24] and Lee *et al.* [25] considered the problem of the elastic interaction between screw dislocations and the blunt crack with a sharp crack. The elastic inter-

*Project supported by the National Natural Science Foundation of China (Grant Nos. 10872065 and 50801025).

†Corresponding author. E-mail: fangqh1327@tom.com

© 2010 Chinese Physical Society and IOP Publishing Ltd

action between a screw dislocation dipole and a sharp crack emanating from a surface semi-elliptic hole is investigated by Yang *et al.*[26] However, the problem of edge dislocations interacting with a crack emanating from a surface semi-elliptic hole has not been studied due to the complexity of the calculation.

In the present paper, we analyse the elastic interaction between an edge dislocation and a sharp crack emanating from a surface semi-elliptic hole by the conformal mapping technique and the complex variable method. The stress intensity factor at the tip of the crack and the image force acting on the edge dislocation are derived. The impact of the morphology of the blunt crack and the position of the edge dislocation on the shielding effect to the crack and the image force is discussed.

2. Problem statement and solution

The current problem is shown in Fig. 1(a). A free surface $x = 0$ contains a semi-elliptic hole whose centre is located at the origin, and A and B are the lengths of the major semi-axis and minor semi-axis of the ellipse, respectively. A sharp crack of length $L-A$ emanates from the semi-elliptic hole along the positive x-axis. An edge dislocation of Burgers vector (b_x, b_y) is located at $z_0 = x_0 + \mathrm{i}y_0$.

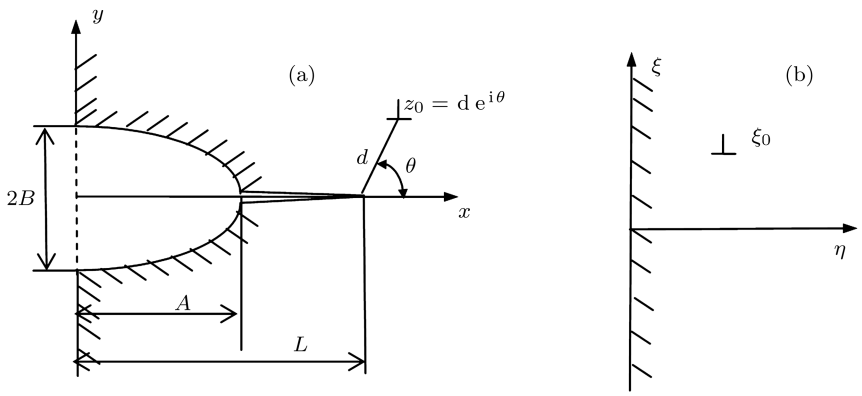


Fig. 1. (a) An edge dislocation near a sharp crack emanating from a semi-elliptic hole. (b) The ζ-plane after conformal mapping.

For the plane strain problem, stress fields and displacement fields can be expressed in terms of two Muskhelishvili's complex potentials $\varphi(z)$ and $\psi(z)$.[27]

$$\sigma_{xx} + \sigma_{yy} = 2[\varphi'(z) + \overline{\varphi'(z)}], \tag{1}$$

$$\sigma_{yy} - \mathrm{i}\sigma_{xy} = \varphi'(z) + \overline{\varphi'(z)} + z\overline{\varphi''(z)} + \overline{\psi'(z)}, \tag{2}$$

$$2\mu(u_x + \mathrm{i}u_y) = \kappa\varphi(z) - z\overline{\varphi'(z)} - \overline{\psi(z)} \tag{3}$$

with $z = x + \mathrm{i}y$ and $\kappa = 3 - 4\nu$, in which μ is the shear modulus and ν is Poisson's ratio. The superposed bar denotes a complex conjugate, and the prime denotes differentiation with respect to the argument z.

Let us introduce the following mapping function[26]

$$z = \omega(\zeta) = \frac{A\sqrt{\zeta^2 + L^2} + B\sqrt{\zeta^2 + L^2 - C^4P^2}}{C^2P} \tag{4}$$

with $\zeta = \eta + \mathrm{i}\xi$, $P = \dfrac{L}{LA - B\sqrt{L^2 - C^2}}$ and $C = \sqrt{A^2 - B^2}$, which maps the surface blunt crack in the z-plane into a half space in the ζ-plane ($\eta > 0$), as shown in Fig. l(b).

With the aid of the mapping function Eq. (4), Eqs. (1) and (2) can be rewritten in the ζ-plane as follows:

$$\sigma_{xx} + \sigma_{yy} = 2[\Phi(\zeta) + \overline{\Phi(\zeta)}], \tag{5}$$

$$\sigma_{yy} - \mathrm{i}\sigma_{xy} = \Phi(\zeta) + \overline{\Phi(\zeta)} + \frac{\omega(\zeta)}{\overline{\omega'(\zeta)}}\overline{\Phi'(\zeta)} + \overline{\Psi(\zeta)}, \tag{6}$$

where $\Phi(\zeta) = \varphi'(\zeta)/\omega'(\zeta)$, $\Phi'(\zeta) = [\varphi''(\zeta)\omega'(\zeta) - \varphi'(\zeta)\omega''(\zeta)]/[\omega'(\zeta)]^2$ and $\Psi(\zeta) = \psi'(\zeta)/\omega'(\zeta)$.

Let us firstly analyse the singularities of the complex potentials. If an edge dislocation is located at an arbitrary point z_0 in the z-plane, the expressions of

the complex potentials $\varphi(z)$ and $\psi(z)$ can be chosen as:

$$\varphi(z) = \gamma \ln(z - z_0) + \varphi_0(z), \tag{7}$$

$$\psi(z) = \bar{\gamma} \ln(z - z_0) - \frac{\gamma \bar{z}_0}{z - z_0} + \psi_0(z), \tag{8}$$

where $\gamma = \dfrac{\mu}{\pi(1+\kappa)}(b_y - \mathrm{i}b_x)$, $\varphi_0(z)$ and $\psi_0(z)$ refer to the terms resulting from the interaction of the edge dislocation with the surface blunt crack.

Substituting Eq. (4) into Eqs. (7) and (8), the complex potentials in the ζ-plane are given as

$$\varphi(\zeta) = \gamma \ln(\zeta - \zeta_0) + \varphi_0(\zeta), \quad \eta > 0, \tag{9}$$

$$\psi(\zeta) = \bar{\gamma} \ln(\zeta - \zeta_0) - \frac{\gamma \overline{\omega(\zeta_0)}}{H_1(\zeta - \zeta_0)} + \psi_0(\zeta), \quad \eta > 0, \tag{10}$$

where

$$H_1 = \frac{1}{C^2 P}\left(\frac{A\zeta_0}{\sqrt{\zeta_0^2 + L^2}} + \frac{B\zeta_0}{\sqrt{\zeta_0^2 + L^2 - C^4P^2}}\right).$$

Applying the Riemann–Schwarz symmetry principle, a new analytic function $\chi(\zeta)$ can be introduced:

$$\chi(\zeta) = \omega(-\zeta)\frac{\varphi'(\zeta)}{\omega'(\zeta)} + \psi(\zeta), \quad \eta > 0. \tag{11}$$

The substitution of Eqs. (9) and (10) into Eq. (11) yields

$$\chi(\zeta) = \frac{H\gamma}{\zeta - \zeta_0} + \bar{\gamma} \ln(\zeta - \zeta_0) + \chi_0(\zeta), \tag{12}$$

where

$$H = -\frac{A\sqrt{\zeta_0^2 + L^2} + B\sqrt{\zeta_0^2 + L^2 - C^4P^2}}{\dfrac{A\zeta_0}{\sqrt{\zeta_0^2 + L^2}} + \dfrac{B\zeta_0}{\sqrt{\zeta_0^2 + L^2 - C^4P^2}}} - \frac{A\sqrt{\bar{\zeta}_0^2 + L^2} + BC\sqrt{\bar{\zeta}_0^2 + L^2 - C^4P^2}}{\dfrac{A\zeta_0}{\sqrt{\zeta_0^2 + L^2}} + \dfrac{B\zeta_0}{\sqrt{\zeta_0^2 + L^2 - C^4P^2}}}.$$

Following Muskhelishvili's treatments, the traction-free boundary condition along the imaginary axis is satisfied by

$$\varphi(\zeta) + \frac{\omega(\zeta)}{\overline{\omega'(\zeta)}}\overline{\varphi(\zeta)} + \overline{\psi(\zeta)} = 0. \tag{13}$$

To treat the boundary conditions on the interface, it is convenient to introduce the following analytic function:

$$\begin{aligned}\Omega(\zeta) &= -\overline{\chi}(-\zeta) \\ &= -\frac{\overline{H}\bar{\gamma}}{-\zeta - \overline{\zeta_0}} - \gamma \ln(-\zeta - \overline{\zeta_0}) + \Omega_0(\zeta), \\ &\quad \eta < 0.\end{aligned} \tag{14}$$

Using Eq. (13) together with Eq. (14), we have

$$\varphi^+(t) - \Omega^-(t) = 0, \tag{15}$$

where t denotes the point on the imaginary axis in the ζ-plane. The superscripts + and − denote the boundary values of a physical quantity when ζ approaches the imaginary axis from $\eta > 0$ and $\eta < 0$, respectively. Considering Eqs. (9) and (14), boundary condition Eq. (15) can be rewritten as:

$$\begin{aligned}\varphi_0^+(t) - \Omega_0^-(t) = &-\gamma \ln(t - \zeta_0) - \frac{\overline{H}\bar{\gamma}}{-t - \bar{\zeta}_0} \\ &-\gamma \ln(-t - \bar{\zeta}_0).\end{aligned} \tag{16}$$

According to the Plemeij formula, we obtain

$$\varphi_0(\zeta) = -\frac{\overline{H}\bar{\gamma}}{-\zeta - \bar{\zeta}_0} - \gamma \ln(-\zeta - \bar{\zeta}_0), \tag{17}$$

$$\Omega_0(\zeta) = \gamma \ln(\zeta - \zeta_0). \tag{18}$$

Substituting Eq. (17) into Eq. (9), the complex potential $\varphi(\zeta)$ is given as

$$\varphi(\zeta) = \gamma \ln(\zeta - \zeta_0) - \frac{\bar{H}\bar{\gamma}}{-\zeta - \bar{\zeta}_0} - \gamma \ln(-\zeta - \bar{\zeta}_0). \tag{19}$$

From Eqs. (14) and (18), the complex potential $\chi(\zeta)$ can be obtained

$$\chi(\zeta) = \frac{H\gamma}{\zeta - \zeta_0} + \bar{\gamma} \ln(\zeta - \zeta_0) - \bar{\gamma} \ln(-\zeta - \bar{\zeta}_0). \tag{20}$$

The substitution of Eqs. (19) and (20) into Eq. (11) yields

$$\begin{aligned}\psi(\zeta) = &\frac{A\sqrt{\zeta^2 + L^2} + B\sqrt{\zeta^2 + L^2 - C^4P^2}}{\dfrac{A\zeta}{\sqrt{\zeta^2 + L^2}} + \dfrac{B\zeta}{\sqrt{\zeta^2 + L^2 - C^4P^2}}}\left(\frac{\gamma}{\zeta - \zeta_0} + \frac{\gamma}{-\zeta - \bar{\zeta}_0} - \frac{\bar{H}\bar{\gamma}}{(-\zeta - \bar{\zeta}_0)^2}\right) \\ &+\frac{H\gamma}{\zeta - \zeta_0} + \bar{\gamma} \ln(\zeta - \zeta_0) - \bar{\gamma} \ln(-\zeta - \bar{\zeta}_0).\end{aligned} \tag{21}$$

In order to validate the analytical results derived in this manuscript, we give the degenerated results. First letting $B = 0$ and $A = L$, then letting $A = 0$, in this case $\zeta = z$ and $\zeta_0 = z_0$, the results given in Eqs. (19) and (21) can be reduced to

$$\varphi(z) = \gamma \ln(z - z_0) - \gamma \ln(-z - \overline{z_0}) + \frac{(z_0 + \overline{z_0})\bar{\gamma}}{-z - \overline{z_0}}, \tag{22}$$

$$\psi(z) = \bar{\gamma} \ln(z - z_0) - \bar{\gamma} \ln(-z - \overline{z_0}) - \frac{\gamma \overline{z_0}}{z - z_0} + \frac{\gamma z}{-z - \overline{z_0}} + \frac{z(z_0 + \overline{z_0})\bar{\gamma}}{(-z - \overline{z_0})^2}. \tag{23}$$

As expected, the stress fields are the same as those obtained by Hirth and Lothe[27] for the case of an edge dislocation near a half-plane.

In view of Eqs. (1)–(6) and the obtained complex potentials in Eqs. (19) and (21), the stress fields and displacement fields can be easily derived. Here we omit the details to save space.

3. Stress intensity factors at the crack tip

Stress intensity factors (SIFs) near crack tips are a very important and meaningful physical quantum. According to Zhang *et al.*,[28] the stress intensity factors at the crack tip can be found from the complex stress field as:

$$\begin{aligned} K_{\mathrm{I}} - \mathrm{i}K_{\mathrm{II}} &= \sqrt{2\pi} \lim_{\zeta \to 0} \sqrt{\omega(\zeta) - \omega(0)}(\sigma_{yy} - \mathrm{i}\sigma_{xy}) \\ &= \sqrt{2\pi} \lim_{\zeta \to 0} \sqrt{\omega(\zeta) - \omega(0)} \left[\frac{\varphi'(\zeta)}{\omega'(\zeta)} + \frac{\overline{\varphi'(\zeta)}}{\overline{\omega'(\zeta)}} + \omega(\zeta) \frac{\overline{\varphi''(\zeta)\omega'(\zeta)} - \overline{\varphi'(\zeta)\omega''(\zeta)}}{\overline{[\omega'(\zeta)]^3}} + \frac{\overline{\psi'(\zeta)}}{\overline{\omega'(\zeta)}} \right] \end{aligned} \tag{24}$$

with

$$\varphi'(\zeta) = \frac{\gamma}{\zeta - \zeta_0} - \frac{\bar{H}\bar{\gamma}}{(-\zeta - \bar{\zeta}_0)^2} + \frac{\gamma}{-\zeta - \bar{\zeta}_0}, \tag{25}$$

$$\varphi''(\zeta) = -\frac{\gamma}{(\zeta - \zeta_0)^2} - \frac{2\bar{H}\bar{\gamma}}{(-\zeta - \bar{\zeta}_0)^3} + \frac{\gamma}{(-\zeta - \bar{\zeta}_0)^2}, \tag{26}$$

$$\psi'(\zeta) = -\frac{H\gamma}{(\zeta - \zeta_0)^2} + \frac{\bar{\gamma}}{\zeta - \zeta_0} + \frac{\bar{\gamma}}{-\zeta - \bar{\zeta}_0} - \frac{\omega(\zeta)}{\omega'(\zeta)}\varphi''(\zeta) + \left[\frac{\omega''(\zeta)\omega(\zeta)}{[\omega'(\zeta)]^2} - 1 \right] \varphi'(\zeta), \tag{27}$$

$$\omega'(\zeta) = \frac{1}{C^2 P} \left(\frac{A\zeta}{\sqrt{\zeta^2 + L^2}} + \frac{B\zeta}{\sqrt{\zeta^2 + L^2 - C^4 P^2}} \right), \tag{28}$$

$$\omega''(\zeta) = \frac{1}{C^2 P} \left(\frac{AL^2}{(\zeta^2 + L^2)^{3/2}} + \frac{B(L^2 - C^4 P^2)}{(\zeta^2 + L^2 - C^4 P^2)^{3/2}} \right). \tag{29}$$

The substitution of Eqs. (25)–(29) into Eq. (24) yields

$$K_{\mathrm{I}} - \mathrm{i}K_{\mathrm{II}} = \sqrt{\pi} \frac{LCP\sqrt{L^2 - C^4P^2}\sqrt{\dfrac{\dfrac{A}{L} + \dfrac{B}{\sqrt{L^2 - C^4P^2}}}{P}}}{LB + A\sqrt{L^2 - C^4P^2}} \left(\frac{\gamma}{-\zeta_0} - \frac{\bar{H}\bar{\gamma}}{\bar{\zeta}_0^2} + \frac{\gamma}{-\bar{\zeta}_0} - \frac{\bar{H}\bar{\gamma}}{\bar{\zeta}_0^2} + \frac{\gamma}{-\bar{\zeta}_0} + \frac{\gamma}{-\zeta_0} \right). \tag{30}$$

Using Eq. (30), Figs. 2 and 3 show the normalized SIF $K_{\mathrm{I}0} = K_{\mathrm{I}}/[\mu\sqrt{b_x + b_y}/\pi(1+\kappa)]$ versus θ(radian) with different values of L/A. It is found that, if $b_y = 0$, the edge dislocation component b_x will shield the tip first, and then anti-shield it with the increment of the absolute value of θ (radian). Therefore, the edge dislocation with Burgers vector (0, b_y) reduces the SIF K_{I} of the crack only when it is located in the certain region. There exists a critical value of θ and the stress intensity factor $K_{\mathrm{I}} = 0$. The shielding effect is maximal around $\theta = 0.6$ and the anti-shielding effect is maximal around $\theta = 2$. It is seen that $K_{\mathrm{I}0}$ is always

negative when $b_x = 0$, which means the edge dislocation with Burgers vector $(0, b_y)$ can always reduce the SIF $K_{\rm I}$ at the tip of the crack (shielding effect). The shielding effect to $K_{\rm I}$ produced by the edge dislocation component b_y is maximal around $|\theta| = 1.1$. The shielding effect to $K_{\rm I}$ decreases with the increment of L/A.

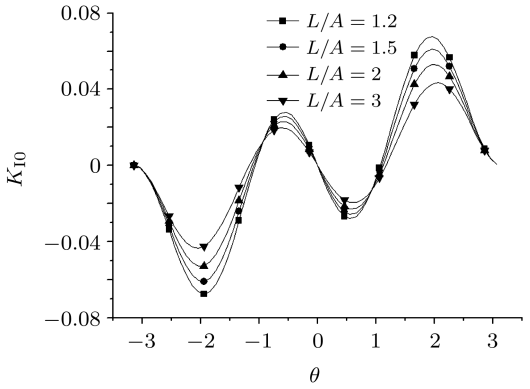


Fig. 2. The normalized SIF $K_{\rm I0}$ versus θ with different L/A for $b_y = 0$, $A/b_x = 10^4$, $B/b_x = 10^3$, $d/b_x = 10^3$.

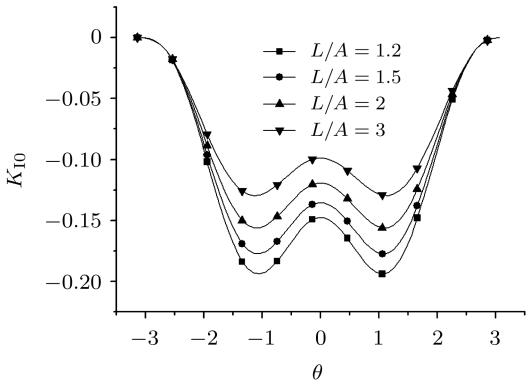


Fig. 3. The normalized SIF $K_{\rm I0}$ versus θ with different L/A for $b_x = 0$, $A/b_y = 10^4$, $B/b_y = 10^3$, $d/b_y = 10^3$.

Figure 4 shows the normalized SIF $K_{\rm I0} = K_{\rm I}/[\mu\sqrt{b_x + b_y}/\pi(1+\kappa)]$ versus $x_0/L(z_0 = x_0 + {\rm i}y_0)$ with different values of B/A. The shielding effect increases with the increase of B/A, but decreases with the increase of x_0/L. In addition, the shielding effect to the SIFs increases acutely when the dislocation approaches the tip of the crack.

The variation of the normalized SIF $K_{\rm II0} = K_{\rm II}/[\mu\sqrt{b_x + b_y}/\pi(1+\kappa)]$ with respect to θ is shown in Figs. 5 and 6 with different values of L/A. It is seen that $K_{\rm II0}$ is always negative when $b_y = 0$, which means the edge dislocation with Burgers vector $(b_x, 0)$ can reduce the SIF $K_{\rm II}$ of the crack (shielding effect). The shielding effect to $K_{\rm II}$ produced by the edge dislocation component b_x is maximal as $\theta = 0$. The shielding effect to $K_{\rm II}$ also decreases with the increment of L/A. It is found that, if $b_y = 0$, the edge dislocation component b_x will shield the tip first, and then anti-shield it with the increment of the absolute value of θ (radian). Therefore, the edge dislocation with Burgers vector $(0, b_y)$ reduces the SIF $K_{\rm II}$ of the crack only when it is located in a certain region. The shielding effect is maximal around $\theta = 0.6$ and the anti-shielding effect is maximal around $\theta = 2$.

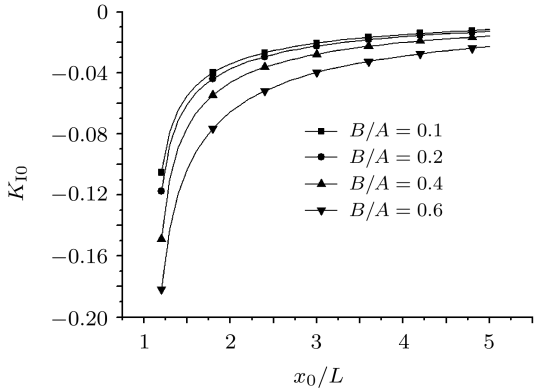


Fig. 4. The normalized SIF $K_{\rm I0}$ versus x_0/L with different B/A for $L/A = 2$, $A/b_y = 10^4$, $b_x = b_y$.

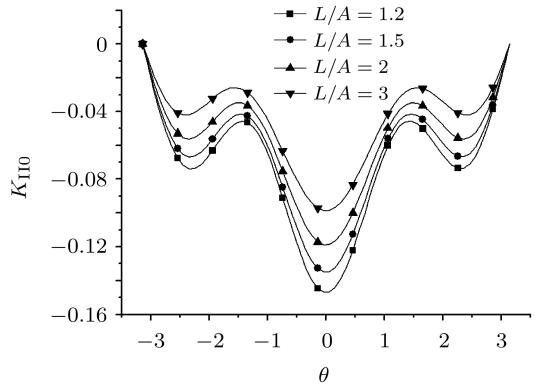


Fig. 5. The normalized SIF $K_{\rm II0}$ versus θ with different L/A for $b_y = 0$, $A/b_x = 10^4$, $B/b_x = 10^3$, $d/b_x = 10^3$.

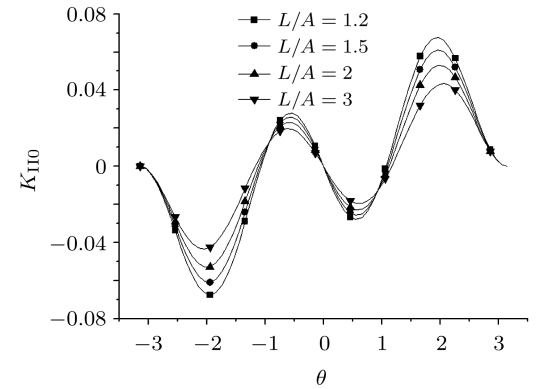


Fig. 6. The normalized SIF $K_{\rm II0}$ versus θ with different L/A for $b_x = 0$, $A/b_y = 10^4$, $B/b_y = 10^3$, $d/b_y = 10^3$.

Figure 7 shows the normalized SIF $K_{\rm II0} = K_{\rm II}/[\mu\sqrt{b_x+b_y}/\pi(1+\kappa)]$ versus $x_0/L(z_0 = x_0 + {\rm i}y_0)$ with different values of B/A. It is also found that the shielding effect to $K_{\rm II}$ increases with the increase of B/A, but decreases with the increase of x_0/L.

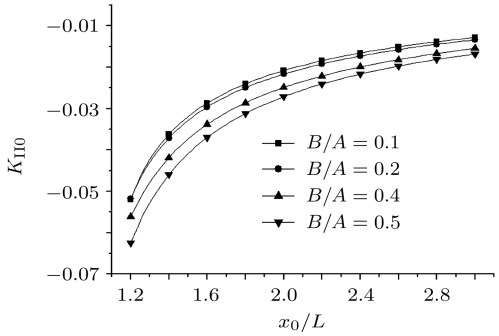


Fig. 7. The normalized SIF $K_{\rm II0}$ versus x_0/L with different B/A for $L/A = 2$, $A/b_y = 10^4$, $b_x = b_y$.

4. Image force on the dislocation

In the current problem, of particular interest is the image force acting on the edge dislocation. Since the elastic strain energy of the system depends on the dislocation position, the unit length of dislocation line is subject to a force (f_x,f_y), which may be calculated through the Peach–Koehler formula:[28]

$$\begin{aligned} & f_x - {\rm i}f_y \\ &= \left[\sigma^*_{xy}b_x + \sigma^*_{yy}b_y\right] + {\rm i}\left[\sigma^*_{xx}b_x + \sigma^*_{xy}b_y\right], \end{aligned} \tag{31}$$

where σ^*_{xx}, σ^*_{yy} and σ^*_{xy} are the perturbation stress fields at the dislocation point. The perturbation stresses can be evaluated by the perturbation complex potentials and the Peach–Koehler formula can be rewritten as

$$f_x - {\rm i}f_y = \frac{\mu(b_y^2+b_x^2)}{\pi(1+\kappa)}\left[\frac{\Phi^*(\zeta_0)+\overline{\Phi^*(\zeta_0)}}{\gamma} + \frac{\overline{\omega(\zeta_0)}\Phi^{*'}(\zeta_0)+\Psi^*(\zeta_0)}{\bar\gamma}\right]. \tag{32}$$

According to the work of Stagni,[29] the perturbation complex potentials $\Phi^*(\zeta_0)$, $\Phi^{*'}(\zeta_0)$ and $\Psi^*(\zeta_0)$ may be calculated as follows:

$$\Phi^*(\zeta_0) = \lim_{\zeta\to\zeta_0}\left[\frac{\varphi'(\zeta)}{\omega'(\zeta)} - \frac{\varphi_0'(\zeta)}{\omega'(\zeta)}\right], \tag{33}$$

$$\Phi^{*'}(\zeta_0) = \lim_{\zeta\to\zeta_0}\left[\frac{\varphi''(\zeta)\omega'(\zeta)-\varphi'(\zeta)\omega''(\zeta)}{[\omega'(\zeta)]^3} - \frac{\varphi_0''(\zeta)\omega'(\zeta)-\varphi_0'(\zeta)\omega''(\zeta)}{[\omega'(\zeta)]^3}\right], \tag{34}$$

$$\Psi^*(\zeta_0) = \lim_{\zeta\to\zeta_0}\left[\frac{\psi'(\zeta)}{\omega'(\zeta)} - \frac{\psi_0'(\zeta)}{\omega'(\zeta)}\right]. \tag{35}$$

With the substitution of Eqs. (25)–(29) into Eqs. (33)–(35), we obtain

$$\Phi^*(\zeta_0) = \frac{-\dfrac{\bar H\bar\gamma}{(-\zeta_0-\bar\zeta_0)^2} + \dfrac{\gamma}{-\zeta_0-\bar\zeta_0}}{\dfrac{1}{C^2P}\left(\dfrac{A\zeta_0}{\sqrt{\zeta_0^2+L^2}} + \dfrac{B\zeta_0}{\sqrt{\zeta_0^2+L^2-C^4P^2}}\right)}, \tag{36}$$

$$\begin{aligned} \Phi^{*'}(\zeta_0) = {} & \frac{-\dfrac{2\bar H\bar\gamma}{(-\zeta_0-\bar\zeta_0)^3} + \dfrac{\gamma}{(-\zeta_0-\bar\zeta_0)^2}}{\left[\dfrac{1}{C^2P}\left(\dfrac{A\zeta_0}{\sqrt{\zeta_0^2+L^2}} + \dfrac{B\zeta_0}{\sqrt{\zeta_0^2+L^2-C^4P^2}}\right)\right]^2} \\ & - \frac{\left(-\dfrac{\bar H\bar\gamma}{(-\zeta_0-\bar\zeta_0)^2} + \dfrac{\gamma}{-\zeta_0-\bar\zeta_0}\right)\left(\left(\dfrac{A(\zeta_0^2+L^2)-A\zeta_0^2}{(\zeta_0^2+L^2)^{3/2}} + \dfrac{B(\zeta_0^2+L^2-C^4P^2)-B\zeta_0^2}{(\zeta_0^2+L^2-C^4P^2)^{3/2}}\right)\right)}{\dfrac{1}{C^4P^2}\left[\left(\dfrac{A\zeta_0}{\sqrt{\zeta_0^2+L^2}} + \dfrac{B\zeta_0}{\sqrt{\zeta_0^2+L^2-C^4P^2}}\right)\right]^3}, \end{aligned} \tag{37}$$

$$\Psi^*(\zeta_0) = \frac{C^2P\bar\gamma}{\left(\dfrac{A\zeta_0}{\sqrt{\zeta_0^2+L^2}} + \dfrac{B\zeta_0}{\sqrt{\zeta_0^2+L^2-C^4P^2}}\right)(-\zeta_0-\bar\zeta_0)}$$

$$+\frac{\left(A\sqrt{\zeta_0^2+L^2}+B\sqrt{\zeta_0^2+L^2-C^4P^2}\right)\left(-\dfrac{2\bar{H}\bar{\gamma}}{(-\zeta_0-\bar{\zeta}_0)^3}+\dfrac{\gamma}{(-\zeta_0-\bar{\zeta}_0)^2}\right)}{\dfrac{1}{C^2P}\left(\dfrac{A\zeta_0}{\sqrt{\zeta_0^2+L^2}}+\dfrac{B\zeta_0}{\sqrt{\zeta_0^2+L^2-C^4P^2}}\right)^2}$$

$$-\left[\frac{C^2P\left(\dfrac{A(\zeta^2+L^2)-A\zeta^2}{(\zeta^2+L^2)^{3/2}}+\dfrac{B(\zeta^2+L^2-C^4P^2)-B\zeta^2}{(\zeta^2+L^2-C^4P^2)^{3/2}}\right)\left(A\sqrt{\zeta_0^2+L^2}+B\sqrt{\zeta_0^2+L^2-C^4P^2}\right)}{\left(\dfrac{A\zeta_0}{\sqrt{\zeta_0^2+L^2}}+\dfrac{B\zeta_0}{\sqrt{\zeta_0^2+L^2-C^4P^2}}\right)^3}\right.$$

$$\left.-\frac{C^2P}{\left(\dfrac{A\zeta_0}{\sqrt{\zeta_0^2+L^2}}+\dfrac{B\zeta_0}{\sqrt{\zeta_0^2+L^2-C^4P^2}}\right)}\right]\left(-\frac{2\bar{H}\bar{\gamma}}{(-\zeta_0-\bar{\zeta}_0)^3}+\frac{\gamma}{(-\zeta_0-\bar{\zeta}_0)^2}\right). \tag{38}$$

Now the detailed expression of the image force can be found by Eq. (32) together with Eqs. (36)–(38).

In the following discussion, we consider the case that an edge dislocation lies on the x-axis ($z_0 = x_0 > L$) and the component of the edge dislocation $b_y = 0$. Figure 8 shows the normalized image force $f_{x0} = f_x\pi(1+\kappa)/\mu(b_x^2+b_y^2)$ versus x_0/L with different values of L/A. It can be found that the normalized image force f_{x0} is always negative, which means the edge dislocation is always attracted by the crack. The attraction force acting on the edge dislocation decreases with the increment of L/A and x_0/L. Figure 9 shows the normalized image force $f_{x0} = f_x\pi(1+\kappa)/\mu(b_x^2+b_y^2)$ versus B/A with different values of L/A and z_0/L. It is seen from Fig. 9 that the attraction force acting on the dislocation increases with the increase of B/A. The attraction force also decreases with the increment of L/A and x_0/L.

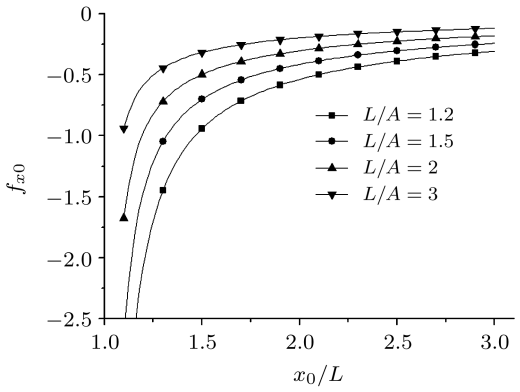


Fig. 8. The normalized image force f_{x0} versus x_0/L with different L/A for $A = 1$, $B = 0.1$, $b_y = 0$.

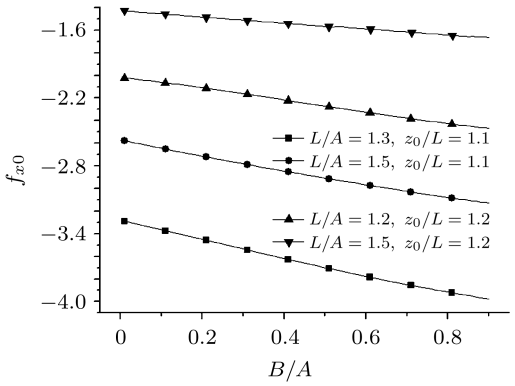


Fig. 9. The normalized image force f_{x0} versus B/A with different L/A and z_0/L for $A = 1$, $b_y = 0$.

5. Conclusions

The problem of an edge dislocation interacting with a sharp crack emanating from a surface semi-elliptic hole is solved by the conformal mapping technique and the complex variable method. Closed form solutions are derived for complex potentials and stress fields. The SIF at the tip of the crack and the image force acting on the edge dislocation are also calculated. The influence of the morphology of the blunt crack and the position of the edge dislocation on the shielding effect to the crack and the image force is discussed.

The results show that the edge dislocation with Burgers vector (0, b_y) can always reduce the SIF $K_{\rm I}$ at the tip of the crack (shielding effect) and the edge dislocation with Burgers vector (b_x, 0) can always reduce the SIF $K_{\rm II}$ at the tip of the crack. The shielding effect of the edge dislocation with Burgers vector (0,

b_y) to the SIF $K_{\rm I}$ occurs only when the dislocation is located in a certain region. Similarly, the shielding effect of the edge dislocation with Burgers vector (b_x, 0) to the SIF $K_{\rm II}$ only occurs when the dislocation is located in a certain region near the crack. The shielding or anti-shielding effect to the SIF increases acutely when the dislocation approaches the tip of the crack. In addition, the effect of the morphology of the crack on the image force on the dislocation is very significant. The attraction force produced by the blunt crack increases with the increase of B/A but decreases with the increase of L/A and x_0/L.

References

[1] Zhang T Y and Li J C M 1992 *J. Appl. Phys.* **72** 2215
[2] Zhang T Y and Tong T 1995 *J. Appl. Phys.* **78** 4873
[3] Lin I H and Thomson R 1986 *Acta Metall.* **34** 187
[4] Long Q W and Liang Y 1984 *Acta Phys. Sin.* **33** 755 (in Chinese)
[5] Shiue S T 1997 *Mater. Chem. Phys.* **48** 220
[6] Zhu T, Li J and Yip S 2004 *Phys. Rev. Lett.* **93** 025503
[7] Fang Q H, Liu Y W and Jiang C P 2003 *Int. J. Struct. Solids* **40** 5781
[8] Fan T Y, Guo R P and Liu G T 2003 *Chin. Phys.* **12** 1149
[9] Jin B, Fang Q H and Liu Y W 2007 *Acta Mech. Solida. Sin.* **20** 50
[10] Tanguy D, Razafindrazaka M and Delafosse D 2008 *Acta Mater.* **56** 2441
[11] Weertman J 1996 *Dislocation Based Fracture Mechanics* (Singapore: World Scientific) p193
[12] Lung C W and Wang L 1984 *Phil. Mag.* **50** L91
[13] Lee S 1987 *Eng. Fract. Mech.* **27** 539
[14] Chen B T, Zhang T Y and Lee S 1999 *Mech. Mater.* **31** 71
[15] Fischer L L and Beltz G E 2001 *J. Mech. Phys. Solids* **49** 635
[16] Qian C F, Chu W Y and Qiao L J 2002 *Int. J. Fract.* **117** 313
[17] Huang M and Li Z 2004 *J. Mech. Phys. Solids* **52** 1991
[18] Li T, Li Z and Sun J 2006 *Scripta Mater.* **55** 703
[19] Song H P, Fang Q H and Liu Y W 2009 *Chin. Phys.* B **18** 1564
[20] Song H P, Fang Q H and Liu Y W 2009 *Chin. Phys. Lett.* **26** 096102
[21] Vehoff H and Neumann P 1979 *Acta Metall.* **27** 915
[22] Ohr S M 1985 *Mater. Sci. Eng.* **72** 1
[23] Shiue S T and Lee S 1988 *J. Appl. Phys.* **64** 129
[24] Shiue S T and Lee S 1989 *Phys. Status Solidi* A **113** 365
[25] Lee S L, Huang W S and Shiue S T 1991 *Mater. Sci. Engng.* A **142** 41
[26] Yang Y S, Lee S L and Lan B T 1995 *Eng. Fract. Mech.* **52** 83
[27] Hirth J P and Lothe J 1983 *Theory of Dislocations* 2nd ed. (New York: McGraw-Hill) p86
[28] Zhang T Y, Tong P, Hao O and Lee S 1995 *J. Appl. Phys.* **78** 4873
[29] Stagni L 1993 *Philos. Mag.* A **68** 49